Fischer, Michael

Structure and bonding of water molecules in zeolite hosts: Benchmarking plane-wave DFT against crystal structure data

Journal Article	as:	published version (Version of Record)
DOI of this document*(secondary publication):		https://doi.org/10.26092/elib/2846
Publication date of this document:		06/03/2024

* for better findability or for reliable citation

Recommended Citation (primary publication/Version of Record) incl. DOI:

Fischer, Michael. "Structure and bonding of water molecules in zeolite hosts: Benchmarking plane-wave DFT against crystal structure data" Zeitschrift für Kristallographie - Crystalline Materials, vol. 230, no. 5, 2015, pp. 325-336. https://doi.org/10.1515/zkri-2014-1809

Michael Fischer*

Structure and bonding of water molecules in zeolite hosts: Benchmarking plane-wave DFT against crystal structure data

Abstract: Density-functional theory (DFT) calculations are widely employed to study the interaction of water molecules with zeolite frameworks. However, there have been only few attempts to assess whether these computations reproduce experimental structure data sufficiently well, especially with regard to the hydrogen positions of the water molecules. In this work, a detailed comparison between experimental crystal structures and DFT-optimised structures is made for six water-loaded natural zeolites. For each system, high-quality structure determinations from neutron diffraction data have been reported (bikitaite/Li–BIK, edingtonite/Ba–EDI, gismondine/Ca–GIS, scolecite/Ca–NAT, natrolite/Na–NAT, yugawaralite/Ca–YUG). Using a plane-wave DFT approach, the performance of six pure and three dispersion-corrected exchange-correlation functionals is compared, focusing on an optimisation of the atomic coordinates in a fixed unit cell (with cell parameters taken from experiment). It is found that the PBE and the PW91 functional give the smallest overall deviation between experiment and computation. Of the dispersion-corrected approaches, the PBE–TS functional exhibits the best performance. For the PBE and PBE–TS functionals, the agreement between experiment and DFT is analysed in more detail for different groups of interatomic distances. Regarding the OW–H distances in the water molecules, the DFT optimisations lead to physically realistic bond lengths. On the other hand, DFT has a systematic tendency to underestimate the length of hydrogen bonds. The cation-oxygen distances are mostly in very good agreement with experiment, although some exceptions indicate the necessity of further studies.

Keywords: benchmarking; computational chemistry; density-functional theory; water adsorption; zeolites.

***Corresponding author: Michael Fischer,** Fachgebiet Kristallographie, Fachbereich Geowissenschaften, Klagenfurter Straße 2, Universität Bremen, 28359 Bremen, Germany, E-mail: michael.fischer@uni-bremen.de

DOI 10.1515/zkri-2014-1809
Received October 9, 2014; accepted December 14, 2014; published online February 12, 2015

Introduction

The structure, bonding, and dynamics of water molecules located in zeolite pores have received continued scientific interest. On the one hand, water-loaded zeolites are well-suited model systems to investigate the behaviour of water under confinement from a fundamental point of view ([1–3] and references therein). On the other hand, the presence of water in zeolite pores also plays an important role in various applications, e.g., in the field of thermal energy storage, where water adsorption/desorption cycles can be used to store and release heat [4–6].

While all-silica zeolites exhibit hydrophobic behaviour [7], zeolites with a charged framework and charge-balancing cations are hydrophilic due to the attractive electrostatic interaction of the cations with the dipolar water molecules. In addition to these ionic bonds, hydrogen bonds to framework oxygens or between neighbouring water molecules determine the equilibrium position of the water molecules. Naturally, these bonds also influence their dynamics. In zeolites with small pores, all water molecules are coordinated to cations, making them relatively immobile. Another type of “free” water has been observed in zeolites with larger pores, such as zeolites A and Y. Simulations have shown that these water molecules possess a significantly higher mobility than the strongly coordinated water molecules [2]. In a recent experimental study of zeolite A, an unexpected type of water clustering in the cages of this structure was observed, highlighting that the application of state-of-the-art techniques can still lead to novel insights, despite decades of previous work [8].

Experimentally, the position and orientation of water molecules in zeolite pores can be determined using neutron diffraction experiments with single crystal samples, preferentially at low temperatures (to reduce dynamic disorder). The ZeoBase database of zeolite-type

crystal structures includes approximately 30 entries of water-loaded zeolites that were determined with this method [9]. However, the actual number of distinct structures is lower, because some systems have more than one entry, e.g., in cases where measurements at different temperatures were carried out.

Electronic structure calculations, e.g., within the framework of density-functional theory (DFT), can provide valuable insights into the properties of water adsorbed in zeolite pores [2, 3, 10, 11]. The range of application of these calculations extends from the prediction of equilibrium geometries to ab-initio molecular dynamics (MD) calculations. Ab-initio MD calculations have been used to study the behaviour of water under confinement, e.g., in small-pore zeolites where the H_2O molecules form one-dimensional chains [12–14] and in different models of zeolite A with hydrophobic and hydrophilic character [3]. Other investigations using this method have addressed the protonation of water in proton-exchanged zeolites [10].

In order to judge the performance of different exchange-correlation functionals, DFT calculations have been benchmarked against high-level wave-function-based calculations for clusters representing key features of the zeolite structure [11]. A similar approach has been employed recently for water interacting with metal-organic frameworks [15, 16]. However, despite the availability of experimental crystal structure data for several water-loaded zeolites, only few computational investigations have assessed the agreement between structures obtained from electronic structure calculations and experimental crystal structures. In particular, Larin and coworkers used periodic Hartree–Fock calculations to study the hydrogen bonding in zeolites containing adsorbed water molecules, and compared some of the resulting bond lengths and angles to available experimental data [17]. Subsequently, the same group of authors proposed a multi-step computational approach to improve the geometries of the adsorbed water molecules [18]: After an initial geometry optimisation using Hartree-Fock or DFT calculations with a minimal basis set, a scaling procedure was used to adjust the bond lengths and angles of the water molecules in order to match results obtained with larger basis sets. Due to the limited availability of exchange-correlation functionals, let alone dispersion-corrected DFT, at the time of that study, it was not assessed to what extent the choice of functional (and possible inclusion of dispersion corrections) affects the resulting geometry.

In this work, DFT geometry optimisations using nine different exchange-correlation functionals (three of them including a dispersion correction term) are performed for a total of six water-loaded zeolites for which a structure determination from neutron diffraction data has been reported in the literature. Because many application-related studies focus on the relaxation of atomic coordinates within a fixed cell, experimental lattice parameters are used in the calculations. In order to assess the performance of the different functionals, the overall deviation between the DFT-optimised structure and the experimental reference structure is calculated from the atomic coordinates for each case. The resulting structures are then discussed in more detail for two of the best-performing functionals, with a focus on (a) intermolecular bonds in the water molecules, (b) hydrogen bonds, and (c) cation-oxygen distances.

Models and methods

Experimental zeolite structures

Experimentally determined zeolite structures with water molecules in the pores were taken from the ZeoBase database [9]. Only structures fulfilling the following criteria were included in the set of reference structures:

- The structure has been determined from single-crystal neutron diffraction data, as this is the most accurate method to determine the positions of hydrogen (or deuterium) atoms of the water molecules.
- The structure does not contain structural disorder or mixed occupancies in the framework and cation sites. In cases where the water molecules are disordered, atoms with low occupancies were removed prior to the DFT calculations.
- The unit cell does not exceed a certain size (all lattice dimensions < 20 Å) in order to render the computations feasible on standard clusters (typical calculations used 16 CPUs and took several hours to a few days to complete).

Based on these criteria, six experimental datasets were identified, for which the framework type as well as the temperature of the measurement (T_{meas}) are listed below:

- **Li–Bikitaite (Li–BIK):** Natural bikitaite, T_{meas} = 13 K [19].
- **Ba–Edingtonite (Ba–EDI):** Natural edingtonite, T_{meas} = 100 K [20].
- **Ca–Gismondine (Ca–GIS):** Natural gismondine, T_{meas} = 15 K [21].
- **Ca–Scolecite (Ca–NAT):** Natural scolecite, T_{meas} = 20 K [22].
- **Na–Natrolite (Na–NAT):** Natural natrolite, T_{meas} = 20 K [23].
- **Ca–Yugawaralite (Ca–YUG):** Natural yugawaralite, T_{meas} = 13 K [24].

Relevant crystallographic information (cell parameters, space group, sum formula) for the six systems are summarised in Table 1. With the exception of Ca–NAT, the standardised cell as given by ZeoBase was used (the standardised cell differs from the cell setting used in the publication for the case of Ca–GIS, but is identical in the remaining four cases).

In some instances, the structures of the zeolites had to be modified prior to the calculations, since the DFT calculations cannot deal with some phenomena that are frequently observed experimentally,

Tab. 1: Space group, sum formula, and lattice parameters of the six zeolites considered in this work. The *k*-mesh used in the calculations is also given.

Li–BIK		
SG: *P*1	$Li_2Al_2Si_4O_{12} \cdot 2H_2O$	2 × 3 × 2 *k*-mesh
a = 8.5971 Å	*b* = 4.9395 Å	*c* = 7.6121 Å
$\alpha = 89.85°$	$\beta = 114.52°$	$\gamma = 90.004°$
Ba–EDI		
SG: $P2_12_12$	$BaAl_2Si_3O_{10} \cdot 4H_2O$	2 × 2 × 3 *k*-mesh
a = 9.536 Å	*b* = 9.649 Å	*c* = 6.496 Å
Ca–GIS		
SG: $P2_1/a$	$CaAl_2Si_2O_8 \cdot 4H_2O$	2 × 2 × 2 *k*-mesh
a = 9.853 Å	*b* = 10.011 Å	*c* = 10.614 Å
c-unique		$\gamma = 86.89°$
Ca–NAT		
SG: *Cc*	$CaAl_2Si_3O_{10} \cdot 3H_2O$	2 × 1 × 2 *k*-mesh
a = 6.516 Å	*b* = 18.948 Å	*c* = 9.761 Å
b-unique	$\beta = 108.98°$	
Na–NAT		
SG: *Fdd*2	$Na_2Al_2Si_3O_{10} \cdot 2H_2O$	2 × 2 × 2 *k*-mesh
a = 18.272 Å	*b* = 18.613 Å	*c* = 6.593 Å
Ca–YUG		
SG: *Pc*	$CaAl_2Si_6O_{16} \cdot 4H_2O$	3 × 2 × 2 *k*-mesh
a = 6.700 Å	*b* = 13.972 Å	*c* = 10.039 Å
b-unique	$\beta = 111.07°$	

such as fractional occupancies and disorder. These modifications are summarised in the following:

- In Li–BIK, the occupancies of the T atoms and the Li atoms, which range between 92% and 105% in the experimental structure, were set to 100%.
- In Ba–EDI, the occupancies of the water molecules and the Ba cation, which range between 82% and 96% in the experimental structure, were set to 100%.
- In Ca–GIS, atoms with occupancies < 50% were removed (oxygen atoms OW5 and OW6 and disordered hydrogen atoms with low occupancies), the occupancies of all other atoms were set to 100%.
- In Ca–YUG, atoms with occupancies < 50% were removed (oxygen atoms OW1A, OW4A, and OW5 and disordered hydrogen atoms with low occupancies), the occupancies of all other atoms were set to 100%.

When applying the modifications described above, it was ensured that the resulting structures are electroneutral. The structures of the zeolites are visualised in the Supporting Information.

Details of DFT calculations

The DFT calculations reported in this work were performed using CASTEP, a code which uses a combination of plane waves and pseudopotentials [25]. Ultrasoft pseudopotentials generated on the fly were employed [26]. In all calculations, the atomic coordinates of all atoms were optimised, whereas the lattice parameters were fixed to the experimental values reported in Table 1. Since it has been well established that some exchange-correlation functionals tend to over- or underestimate the lattice parameters considerably in many instances (see e.g., [27] and references therein), it is often preferred to fix the lattice dimensions to accurate experimental values where these are available. This approach has been followed, for example, in various MD studies of the dynamics of water molecules adsorbed in zeolites [10, 12–14]. Thus, there is considerable scope for assessing the performance of different functionals in the prediction of atomic positions without simultaneous optimisation of the lattice parameters. The benchmarking reported here will concentrate on the optimisation of atomic coordinates in a fixed cell.

Initial tests for Li–BIK were performed in order to assess the dependence of the results on the energy cutoff and the size of the *k*-mesh. A cutoff of 800 eV was found to be sufficient (the geometry did not change significantly when increasing the cutoff from 700 eV). However, a dependence of the final structure on the size of the *k*-mesh was observed. Tests with three different *k*-meshes were performed for all zeolites. In many instances, the optimisation using only the gamma-point delivered geometries that deviated from those obtained with larger *k*-meshes, with deviations in some atomic positions of up to 0.1 Å. However, when increasing the *k*-mesh beyond the gamma-point, the geometries usually converged very quickly. The *k*-meshes given in Table 1, which were used in all following calculations, were found to deliver converged geometries.

In order to test the dependence of the resulting geometry on the exchange-correlation functional, six functionals without dispersion correction were included:

- **LDA:** The local density approximation, which uses only local information on the electron density, corresponds to the simplest functional considered [28].

LDA is known to have a tendency towards "overbinding", which manifests itself by an underestimation of equilibrium bond lengths and lattice parameters. Incorporation of information on the electron density gradient (GGA = generalised gradient approximation) can improve upon this behaviour. The following two functionals are "traditional" GGA-type functionals:

- **PW91:** GGA parameterisation by Perdew and Wang ([29] and references therein];
- **PBE:** Re-derivation of GGA by Perdew, Burke, and Ernzerhof [30], simplified with respect to PW91, a very popular functional, especially for solids.

It has been found that these GGA functionals cure some of the mentioned shortcomings of LDA, however, they tend to overestimate equilibrium lattice parameters and related properties, and underestimate surface energies [31]. A number of more recent GGA parameterisations have attempted to overcome these shortcomings. Three of these functionals are considered in this work:

- **PBEsol:** GGA-type functional based on PBE that is specifically designed for solids [31], gives better lattice parameters, but less accurate atomisation energies than PBE;
- **WC:** Similar parameterisation as PBEsol [32], delivers improved prediction of lattice parameters in comparison to PBE;
- **RPBE:** Revised version of PBE that is designed to deliver more accurate atomisation energies and chemisorption energies than PBE [33].

Additionally, three different dispersion correction schemes were evaluated:

- **PW91–OBS:** Combination of the PW91 functional with the dispersion correction scheme proposed by Ortmann, Bechstedt, and Schmidt [34]; the dispersion coefficients are based on the

London formula, using experimental polarisabilities and ionisation potentials;
- **PBE–D:** Combination of the PBE functional with the dispersion correction suggested by Grimme [35]; the dispersion coefficients are also calculated using the London formula, but from DFT-calculated polarisabilities and ionisation potentials;
- **PBE–TS:** Combination of the PBE functional with the dispersion correction developed by Tkatchenko and Scheffler [36]; in this method, the dispersion coefficients for each atom are weighted according to the effective volume of the atom in a molecule or solid as calculated from the DFT electron density, using the free atom as the reference state.

As a final remark to this section, we acknowledge that only a limited choice of functionals is included in this study, primarily due to technical limitations. For example, hybrid functionals, which have become popular even for calculations for periodic structures [37], are missing. However, for the foreseeable future, GGA-type functionals will continue to play a very important role, especially for systems with large unit cells, for surfaces, and for ab-initio MD calculations. In many instances, the computationally inexpensive GGA-type functionals might constitute the only possible choice for such investigations. Therefore, a careful benchmarking of the performance of these functionals against experimental data is very important.

Results and discussion

Analysis of deviations in the atomic coordinates

Initially, we assess the agreement between the DFT-optimised structures and experimental data by comparing the atomic coordinates. To do so, we first define a difference vector, which corresponds to the "displacement" of the *i*-th atom in the DFT-optimised structure with respect to the reference position in the experimental structure. This displacement can be expressed as a coordinate triplet (Δx_i, Δy_i, Δz_i). For the case of an orthorhombic structure, the length (modulus) of the difference vector is defined as follows:

$$|\vec{v}_i| = \sqrt{(\Delta x_i \cdot a)^2 + (\Delta y_i \cdot b)^2 + (\Delta z_i \cdot c)^2}$$

In order to express the deviations for all N non-equivalent atoms (or a subset of atoms, e.g., all hydrogen atoms) as a single value, we then take the arithmetic mean of the moduli of the individual difference vectors to get the average positional deviation *dev* (in Ångström):

$$dev = \frac{1}{N} \sum_{i}^{N} |\vec{v}_i|$$

In four of the structures, all atoms are located on general positions. In the remaining two systems, Ba-EDI and Na–NAT, two/one atom/s are located on special positions, while all others occupy general positions. For these two cases, the contributions from the individual atoms were weighted according to their site multiplicity in the calculation of the average positional deviation.

Table 2 reports the values of *dev* for the six zeolites and nine functionals considered. The deviations range from 0.022 Å to 0.230 Å, spanning almost exactly one order of magnitude. While an average agreement of DFT-predicted and experimental positions within ~0.02 Å can be considered as very good, a deviation of more than 0.1 Å is clearly unacceptable. When looking at the individual systems, rather small deviations (mostly below 0.05 Å) are found for Li–BIK, Ba.EDI, Ca–NAT, and Na–NAT, those systems for which the experimental structures were used as input for the calculations without major modifications (apart from an adjustment of some occupancy factors). It is not surprising that the deviations are larger for the remaining two systems, where some disordered atoms had to be removed.

In order to analyse the performance of the different functionals, we use two different approaches: Firstly, we normalise the average positional deviations. For each

Tab. 2: Average positional deviations of DFT-optimised structures with respect to experimental data. All values are given in Å. Deviations above 0.05 Å are highlighted in italics. The value for Ba–EDI and the PBE–D functional is missing because no parameters for barium are available for this dispersion correction scheme [35].

	LDA	PW91	PBE
Li–BIK	0.039	0.026	0.027
Ba–EDI	*0.061*	0.025	0.035
Ca–GIS	*0.098*	*0.063*	*0.060*
Ca–NAT	*0.060*	0.024	0.023
Na–NAT	0.044	0.024	0.022
Ca–YUG	*0.230*	*0.093*	*0.067*
	PBEsol	**WC**	**RPBE**
Li–BIK	0.025	0.026	0.048
Ba–EDI	0.040	0.041	0.042
Ca–GIS	*0.078*	*0.079*	*0.067*
Ca–NAT	0.036	0.037	0.032
Na–NAT	0.025	0.028	0.040
Ca–YUG	*0.123*	*0.123*	*0.074*
	PW91–OBS	**PBE–D**	**PBE–TS**
Li–BIK	0.042	0.032	0.027
Ba–EDI	0.043	n/a	0.044
Ca–GIS	*0.086*	*0.061*	*0.051*
Ca–NAT	0.035	0.036	0.024
Na–NAT	0.027	0.046	0.037
Ca–YUG	*0.160*	*0.093*	*0.065*

zeolite considered, this is achieved by dividing the *dev* values reported in Table 1 by the deviation obtained with the PBE functional (in principle, any functional could be chosen as a reference, but we will see in the following that the PBE functional is a convenient choice). This normalisation allows us to discuss the relative performance of all other functionals with respect to PBE. These normalised positional deviations are displayed in Figure 1.

In the second approach, the positional deviation is averaged over all six zeolites by taking the arithmetic mean of the *dev* values of Table 1. In addition to the global mean deviation *mdev*, analogous values are calculated for separate groups of atoms: Hydrogen atoms (*mdev*[H]), oxygen atoms of water molecules (*mdev*[OW]), cations (*mdev*[cation]), and framework atoms (*mdev*[framework]). These mean deviations are visualised in Figure 2.

Figure 1 shows that, although some functionals outperform the PBE functional for one or two systems, none of them leads to a general improvement over the PBE results across the set of zeolites studied. This is corroborated by the data displayed in Figure 2, which shows that the PBE functional exhibits the lowest mean deviation for most groups of atoms (except for the cation positions, where PW91 and PW91–OBS perform somewhat better). Regarding the other eight functionals, it is quite apparent that the LDA gives the highest deviations for the majority of zeolites. The deviations are largest for the positions of the water molecules, with *mdev*[H] and *mdev*[OW] both exceeding 0.15 Å. While we will not discuss the results for this functional in much detail due to its unsatisfactory performance, the inspection of selected interatomic distances reveals that LDA tends to drastically underestimate

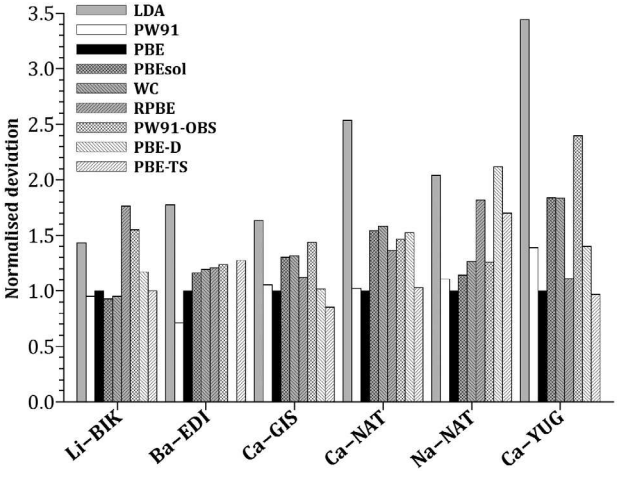

Fig. 1: Average positional deviations for the nine exchange-correlation functionals considered, normalised by the positional deviation obtained with the PBE functional (*dev(PBE)* ≡ 1).

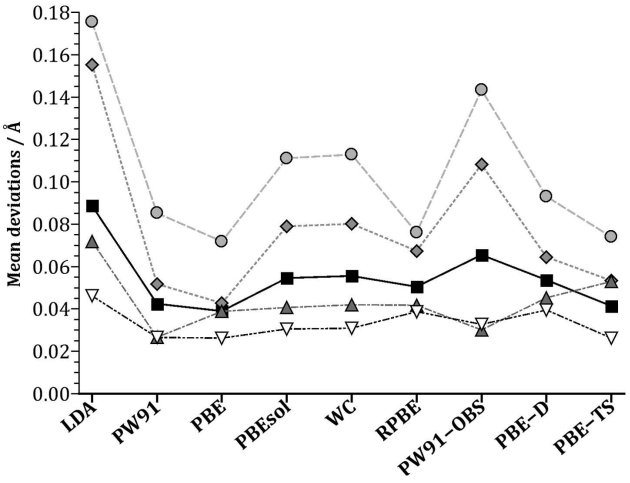

Fig. 2: Global mean deviations calculated for different groups of atoms: Squares = *mdev* for all atoms, circles = *mdev*[H], diamonds = *mdev*[OW], upright triangles = *mdev*[cation], inverse triangles = *mdev*[framework].

the length of hydrogen bonds, often by several per cent. This is in line with previous observations of a severe "overbinding" in calculations using this functional ([38] and references therein). This overbinding is related to the fact that LDA does not incorporate any information on the density gradient, rendering its unsuitable for systems with a strong variation of the electron density [32]. Since the spatial distribution of the electron density in the zeolite structures (and porous materials in general) exhibits large variations (see below), LDA is not a good choice for these materials. The PW91 functional leads to very similar overall deviations as PBE for most systems, but performs considerably better for Ba–EDI, and considerably worse for Ca–YUG. In particular, the mean deviation of the cation positions is significantly lower than for PBE, but it is roughly the same amount higher for the hydrogen atoms. As the PW91 and PBE functionals are closely related derivations of the generalised gradient approximation, it is not surprising that the two functionals show a similar performance in most instances.

Of the recently developed GGA-type functionals, PBEsol and WC exhibit a virtually identical performance. This is well visible in both Figures 1 and 2. The similar behaviour of these two functionals is not surprising, given that they were both designed to improve upon the behaviour of PBE for compact solids [31, 32]. The mean deviations are generally higher than for PBE/PW91. The RPBE functional performs well for hydrogen positions, but, on a whole, also leads to larger positional deviations than PBE. In contrast to PBEsol and WC, the RPBE functional was developed for an improved description of systems with pronounced

density variations, particularly for the chemisorption of molecules on surfaces [33]. Tentatively, the rather modest performance of the three more recent GGA functionals may be attributed to the different degrees of density variation in the zeolite structures: While the density along intra-framework contacts varies only slowly, much more pronounced variations occur near the pore surface, especially in the environment of cations and water molecules. Therefore, the two functionals optimised for solids should give a realistic description of the denser parts of the zeolite structure, but exhibit a less satisfactory performance with regard to the extra-framework species. Indeed, Figure 2 shows that the largest positional deviations for these functionals arise for the water molecules. The opposite is true for RPBE, which gives rather large deviations for the framework atoms, but relatively accurate water positions. It thus appears that neither the functionals that were optimised for solids, nor the functional designed for surfaces, arrive at a better overall description of these systems than the traditional GGA functionals, which were not parameterised specifically for small or large density gradients. The wider implications of this preliminary finding should be investigated in more detail in future studies.

On another note, it has to be considered that one primary aim in the development of PBEsol and WC was the improvement of the prediction of lattice parameters in comparison to PBE [31, 32]. Thus, if a cell optimisation was included in the DFT calculations, they might exhibit a better performance. In this context, it is worth mentioning that both PBEsol and the dispersion-corrected PBE-D functional were found to predict the lattice parameters of various sheet silicates very well [39]. However, as we are only interested in the DFT optimisation of atomic positions in a fixed cell in the context of this study, we leave this topic to future work.

Regarding the dispersion-corrected functionals, it is quite clear that none of the three functionals improves upon the performance of their uncorrected counterparts. Given the fact that dispersion interactions can be expected to play only a minor role in these systems, where covalent and ionic bonds are dominant, this is not entirely surprising. However, the different performance of the three functionals is worth noting: While PW91–OBS and PBE–D give considerably higher deviations than PW91 and PBE, PBE–TS provides an agreement with experiment that is, in most cases, comparable to PBE (with the exception of Na–NAT). The better performance of PBE–TS can be rationalised with the use of weighted dispersion coefficients, as opposed to purely generic dispersion coefficients in PW91–OBS and PBE–D. In the sense of ongoing method development, it is encouraging to see that the most elaborate scheme delivers more accurate results.

The following discussion will focus on PBE and PBE–TS, as these two functionals appear as the most suitable choices to reproduce experimental crystal structures data (PW91 would be an alternative possibility, but we prefer PBE due to the better prediction of hydrogen positions). First, we will look at the geometries of the adsorbed water molecules, and the hydrogen bonds from a global point of view (summarising the results for all six zeolites). Afterwards, we will discuss the environment of the cations separately for each structure. All interatomic distances that are relevant to the following discussion, as well as the optimised structures obtained with the PBE and the PBE–TS functionals, are given in the Supporting Information.

Analysis of interatomic distances for PBE and PBE–TS functionals

Geometry of water molecules

The experimentally measured OW–H bond lengths in the water molecules mostly fall between 0.96 and 0.98 Å, although there are some outliers, primarily for the systems Ba–EDI (three OW–H bonds below 0.95 Å) and Ca–YUG (three OW–H bonds below 0.95 Å and one above 1.0 Å). In the DFT-optimised structures, the bonds have a somewhat higher mean bond length, between 0.98 and 0.99 Å, and the outliers disappear. This is visualised in Figure 3 (as PBE and PBE–TS deliver virtually identical distances, only the PBE data are included in the figure). It has been shown that experimentally observed OW–H distances in

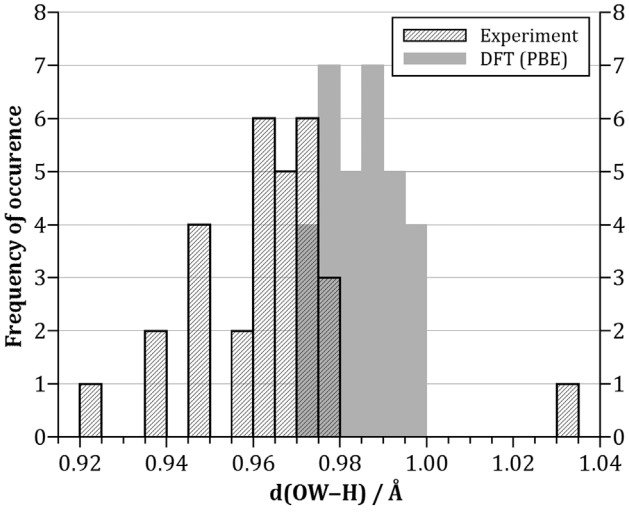

Fig. 3: Histogram plot of the frequency of occurrence of OW-H distances in experimental structures and DFT-optimised structures (PBE functional).

water need to be corrected for thermal ("riding") motion [40]. This correction has been discussed in three of the experimental studies from which the reference structures were taken [19, 22, 23], however, the published structural parameters do not include this correction. In these studies, the correction typically increases the distances by 0.02–0.03 Å, to values around 0.99 Å. These corrected distances are in excellent agreement with the OW-H distances obtained from DFT. Therefore, DFT could be employed to calculate improved OW–H bond distances in cases where a crystal structure refinement delivers unphysical bond lengths, an approach proposed previously by Larin and co-workers [18].

The H–OW–H angles predicted by the calculations are mostly in good agreement with the experimental values. Experimental angles vary from 99 to 111 degrees, and the calculated angles range between 103 and 111 degrees. Again, values obtained with the PBE and PBE–TS functionals are very similar. For four systems (Li–BIK, Ca–GIS, Ca–NAT, Na–NAT), the deviations between calculated and experimental H–OW–H angles do not exceed 1.2 degrees. Larger deviations from 2 to 6 degrees are observed for Ba–EDI, where the experimentally observed angles are more strongly influenced by thermal motion due to the higher measurement temperature, and for the water molecules OW3 and OW4 in Ca–YUG. For these two water molecules, hydrogen disorder was included in the experimental structure refinement, and it is therefore not surprising that the DFT optimisation (without disorder) converges to somewhat different angles.

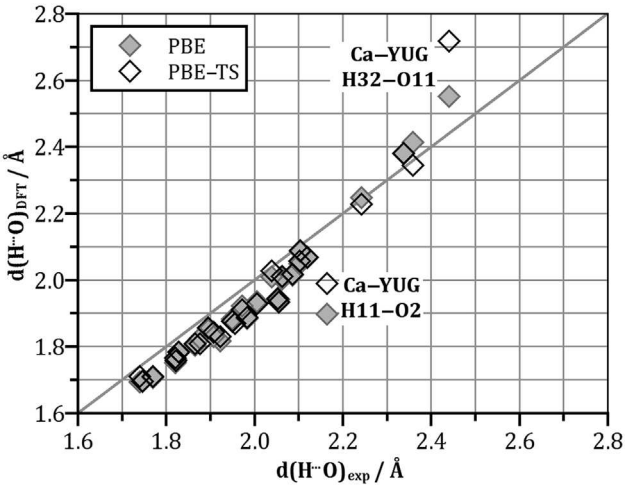

Fig. 4: Plot of H···O distances in the structures optimised with the PBE and PBE–TS functional versus the experimentally observed distances. The straight line, which would correspond to perfect agreement between experiment and calculation, is included to guide the eye. The two cases for which the largest deviations are observed are labelled.

Hydrogen bonds

In addition to the intramolecular OW–H distances, it is of particular interest to assess how well the DFT calculations reproduce the hydrogen bond distances. In this context, we consider all intermolecular H···O contacts that are significantly shorter than 2.5 Å in the experimental structures. This arbitrary threshold value is chosen for mere convenience, and we do not attempt to discuss the actual presence and/or strength of the hydrogen bonds. In the six structures, there are only three hydrogen atoms which do not participate in a hydrogen bond with a length below 2.5 Å: H11 and H21 in Li–BIK and H12 in Ca–YUG.

Figure 4 shows a plot of the H···O distances in the DFT-optimised structures (PBE and PBE–TS) versus the experimentally measured distances. The plot shows a moderate, but systematic underestimation of the hydrogen bond distances for contacts below approximately 2.1 Å for both functionals considered. The deviations range between 0.01 and 0.12 Å, and are thus, on average, significantly larger than the differences in the intramolecular OW–H bond lengths. Thus, these deviations cannot be explained with the correction for thermal motion alone, and must be considered as a systematically occurring feature of the DFT calculations. A comparative underestimation of the hydrogen bond distances has been observed, e.g., in a previously reported investigation on molecular systems which used the PBE functional [38]. It is not surprising that similar deviations occur in periodic structures, and it cannot be expected that the TS dispersion correction (which is strongly damped at these short distances) will qualitatively change the behaviour.

For three of the hydrogen bonds that are longer than 2.1 Å, good agreement is observed, and there seems to be no systematic error. However, there are also two outliers, explicitly labelled in Figure 4, which will be discussed in more detail in the following. To start with, it is worth noting that both outliers are observed in Ca–YUG, and that they are related to water molecules which are disordered in the experimental structure. We first consider the H11···O2 bond, for which the DFT-predicted distances are much shorter than the experimental distance. The hydrogen atom H11 is bonded to the oxygen atom OW1, and an alternative oxygen position OW1A has been reported in the experimental structure (see Figure 5). While this water molecule shares one hydrogen atom (H12) with OW1, the second hydrogen atom H13 points in the opposite direction as H11, forming a hydrogen bond with framework oxygen

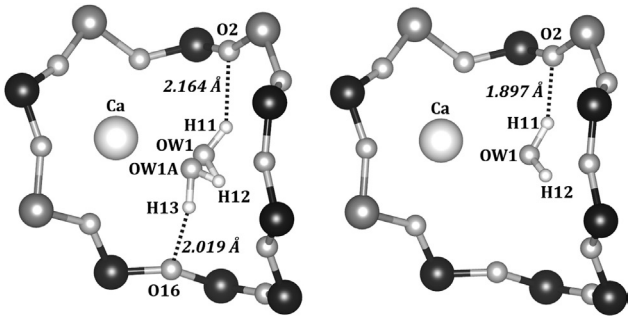

Fig. 5: Environment of the water molecule OW1 in Ca–YUG in the experimental structure (left) and in the DFT-optimised structure (right, PBE functional). Hydrogen bonds are indicated as dashed lines. Other water molecules are omitted for clarity. In the experimental structure, the secondary positions OW1A and hydrogen H13 have an occupancy of less than 20%, whereas the occupancies of sites OW1, H11, and H12 amount to approximately 80%. Figure prepared using Vesta [41].

O16. Apparently, there are two adjacent local minima for the water molecule, both of which will be occupied with a certain probability. The deviations between DFT-optimised structures and experiment can be explained, albeit tentatively, by the difficulties to accurately determine the position of the hydrogen atoms from experimental diffraction data in this complex case.

The DFT calculations predict a significantly longer H–O distance in comparison to experiment for the other outlier highlighted in Figure 4, the H32···O11 bond. Despite the qualitative differences, the reasons for the discrepancy are probably similar to those discussed above: For water molecule OW3, three different hydrogen positions were refined from the experimental data, of which H31 and H32 have similar occupancies (48% and 42%; note that H31, rather than H32, was removed prior to the DFT calculation due to the very short OW3–H31 bond of 0.90 Å). In the light of the disorder and rather low occupancy of H32, it seems reasonable to attribute part of the observed deviations to inaccuracies in the experimental determination of the hydrogen position.

Cation-oxygen distances

In this subsection, the distances between the cations and surrounding oxygen atoms in the DFT-optimised structures are compared to the corresponding distances in the experimental structures. The discussion considers the whole coordination environment of the cations, including framework oxygens and oxygen atoms of the water molecules. Because typical cation-oxygen distances range between 2 and 3 Å, deviations of ~0.02 Å correspond to an error of less than 1%. Deviations on this order will only be mentioned summarily, and the discussion will focus on cases where significantly larger differences are observed.

In Li–BIK, the two non-equivalent lithium cations are tetrahedrally coordinated by three framework oxygens and one water molecule. The interatomic distances between cations and framework oxygens are in excellent agreement with experiment in the structures optimised with the PBE the PBE–TS functional. The cation-OW distances also agree reasonably well, only the Li2–O27 distances is somewhat larger in the DFT-optimised structures (0.02–0.03 Å).

The barium cations in Ba–EDI are tenfold coordinated by six framework oxygen atoms and by four water molecules. Because the cations lie on a twofold rotation axis, there are only five non-equivalent contacts. The distances to the framework oxygens are 0.1–0.25 Å longer than those to water oxygens in the experimental structure, a pronounced, systematic difference that is not observed in any other zeolite studied. This trend is further enhanced in the DFT-optimised structures, where the cation-oxygen distances in the DFT-optimised structures are 0.02–0.04 Å longer for the contacts to framework oxygens, and 0.03–0.05 Å shorter for the contacts to the water molecules. A more detailed analysis of the positional changes of the individual atoms shows that this is primarily caused by a displacement of the Ba atom towards the centre of the pore (along the *c*-axis) by ~0.08 Å (Figure 6). Because the experimental structures measured at 100 K and 293 K show no systematic variation in the Ba–O distances [20], it appears unlikely that this discrepancy stems from the absence of thermal vibrations in the DFT calculations. While we cannot offer an explanation for the observed

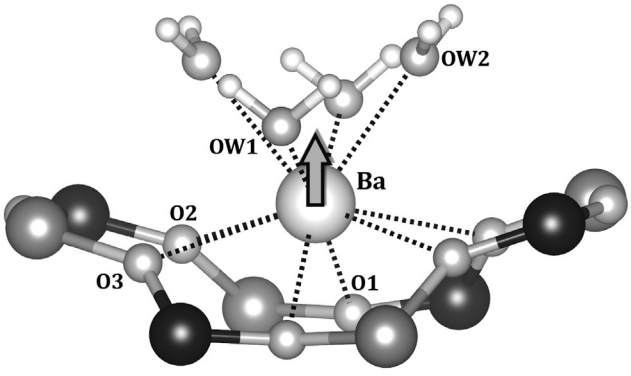

Fig. 6: Environment of the barium cation in Ba–EDI. Cation-oxygen contacts are shown as dashed lines. The direction of the cation displacement in the PBE and PBE–TS structures with respect to the experimental structure is indicated by an arrow. Figure prepared using Vesta [41].

deviation at this stage, it is worth noting that the structure optimised with the PW91 functional exhibits a much better agreement of the barium position with experiment than the PBE and PBE–TS structures (as is visible in Figure 1, Ba–EDI is the only system for which PW91 performs significantly better than PBE). Future studies on Ba-containing compounds could investigate whether this is a systematic feature of the functionals in question.

The calcium cations in Ca–GIS are sixfold coordinated by two framework oxygen atoms and four water molecules. The agreement of the interatomic distances in the DFT-optimised structures with experiment is very good for three of the oxygen atoms, and moderate deviations between 0.02 and 0.04 Å are observed for two others (O8 and OW1). The largest differences occur for the oxygen atom OW4, where the very short Ca–OW4 contact of 2.21 Å in the experimental structure is elongated to 2.27 Å in the DFT-optimised structures. This atom belongs to a water molecule which has an occupancy of approximately 70%, which is replaced by two other water molecules (OW5 and OW6) in the experimental structure in 30% of the cases. It was already pointed out in the original publication that the Ca–OW4 distance is unusually short when compared to crystalline hydrates [21]. Again, we cannot offer a conclusive explanation for the observed differences, but it is worth highlighting that the most significant deviations occur for a cation-oxygen distance that is affected by disorder in the real zeolite, not entirely dissimilar to our previous observations for some of the hydrogen bond distances in Ca–YUG.

In Ca–NAT, the cations are sevenfold coordinated by four framework oxygens and three water molecules. In the structure optimised with the PBE functional, agreement with the experimental distances is excellent for all contacts. Slightly larger deviations are observed for the PBE–TS structure, where two contacts to framework oxygens are 0.02–0.03 Å longer than in the experimental structure.

Na–NAT is the system where the most pronounced differences between the PBE functional and the dispersion-corrected PBE–TS functional occur. In this system, the sodium cations are sixfold coordinated by four framework oxygens and two water molecules. Agreement between DFT and experiment is excellent for the PBE functional, where all Na–O contacts predicted by DFT deviate less than 0.02 Å from the experimental values. Interestingly, a systematic deviation is observed in the PBE–TS structure, where all four shorter Na–O contacts (< 2.4 Å in the experimental structure) are elongated by 0.02–0.06 Å. A closer look at the atomic coordinates reveals that the sodium cation is displaced by 0.06 Å from the experimentally observed position in the PBE–TS structure. This observation points to an unrealistically large influence of the additional long-range interactions provided by the TS correction scheme on the cation location. As Na–NAT is the only sodium-containing system, it remains to be seen whether such problems occur more frequently when applying the Tkatchenko-Scheffler correction scheme to systems that incorporate Na cations.

The calcium cations in Ca–YUG are eightfold coordinated by four framework oxygen atoms and four water molecules. The water molecules OW1 and OW4 are disordered in the experimental structure, with secondary oxygen positions OW1A and OW4A, and the hydrogen atoms of OW3 are also disordered. Despite this rather high degree of disorder (at least in comparison to the other systems studied in this work), the agreement of the DFT-optimised and experimental cation-oxygen distances is mostly very good: For six oxygen atoms, the differences are below or close to 0.02 Å. The exceptions are the water oxygen atoms OW2 and OW4, for which deviations up to 0.04 Å occur.

Further considerations

Finally, it may be remarked that we have not assessed the performance of the DFT calculations in predicting the intra-framework bond lengths and angles (Si–O and Al–O bonds, T–O–T angles). However, Figure 2 shows that the deviations of the coordinates are usually very small for the framework atoms. Furthermore, due to the three-dimensional connectivity of the framework, the capability to completely relax these bonds remains limited as long as the lattice parameters are fixed. The situation changes when a relaxation of the lattice parameters is included in the geometry optimisation, and a careful analysis of the intra-framework bond lengths could aid the identification of systematic errors in this case.

Before presenting some concluding remarks, it is necessary to briefly discuss the inherent limitations of the chosen approach: In the first part of the results section, we have selected the best-performing functionals by a direct comparison of the DFT-optimised structures to experimental data, neglecting any possible errors in the experimental structures. On the other hand, the following discussion showed that this aspect cannot be ignored entirely, and that experimental errors must be invoked to explain some observations, such as the rather large variation of OW–H bond distances in the experimental structures, some of which are unphysical. It could now be asked whether this invalidates our previous conclusions: Could it be possible that those functionals which give the best agreement with experiment primarily reproduce systematic experimental errors most closely? This interpretation can be

discarded when it is considered that these functionals exhibit the best performance across the board, both with regard to the different zeolite structures studied and the different atom types (Figures 1 and 2). Thus, there is good reason to expect that the general conclusions regarding the best functionals would remain valid if an "error-free" set of experimental reference structures was available. For future work, it will be interesting to use high-level wavefunction based methods, which have become available for periodic systems only recently [42], for the geometry optimisations, and compare the resulting structures to both experimental and DFT data.

Conclusions

The comparison of nine exchange-correlation functionals revealed that the two "traditional" GGA functionals PBE and PW91 outperform the more recently developed PBEsol, WC, and RPBE functionals in the prediction of the atomic coordinates when the target is a minimisation of the positional deviations between experimental reference structure and DFT-optimised structure. LDA performs poorly, and while the inclusion of dispersion interactions using generic dispersion coefficients (PW91–OBS, PBE–D) worsens the performance, the PBE–TS functional gives an agreement that is relatively close to PBE for most cases. When looking at the positional deviations in absolute terms, we note that the deviations for most of the functionals (with the exception of LDA) are moderate, remaining below 0.05 Å for those zeolites in which disorder does not play a role (Li–BIK, Ba–EDI, Ca–NAT, Na–NAT). This behaviour is very encouraging when we consider that a variety of different interactions determine the equilibrium structure in these complex systems (covalent bonds between framework atoms, ionic bonds between cations and framework/water molecules, hydrogen bonds). While we have not included the optimisation of the lattice parameters, previous works indicate that dispersion-corrected functionals or functionals developed particularly for solids (PBEsol, WC) tend to exhibit a better performance than PBE/PW91 when these additional degrees of freedom are incorporated [27, 39], which is in accordance with the intention behind the development of these functionals. Nevertheless, calculations using a fixed cell with experimental lattice parameters will remain the method of choice in many instances. For such cases, our study delivers PBE as the recommended choice, while PBE–TS constitutes a suitable alternative when the inclusion of dispersion interactions is important, e.g., in systems that also contain other guest molecules which interact more weakly than water.

The more detailed analysis of the results for the PBE and PBE–TS functionals revealed that the DFT calculations lead to a narrow distribution of the intramolecular OW–H bond lengths. The predicted distances are in excellent agreement with high-quality experimental values that have been corrected for thermal motion, highlighting the capabilities of DFT to predict the geometries of adsorbed water molecules reliably in cases where a refinement from experimental data delivers unsatisfactory results. The situation is different for the hydrogen bonds, where a systematic underestimation of the bond distances is observed in the DFT-optimised structures. As discussed above, this behaviour has been reported previously for the PBE functional, and it is worth noting that all GGA functionals considered in this work lead to similar deviations. It would be desirable to include a selection of more elaborate exchange-correlation functionals (meta-GGA, hybrid functionals) in future studies, as has been done for hydrogen-bonded molecular systems [43, 44]. Regarding the cation-oxygen distances, only marginal deviations between experimental and DFT-optimised structures have been observed for the majority of cases. Some of the discrepancies, such as those seen for the environment of barium in Ba–EDI, deserve further careful study, as various factors might influence the outcome of the computation (e.g., in addition to the exchange-correlation functional, the choice of the pseudopotential will also have a non-negligible impact).

The present study has shown the capabilities of plane-wave DFT using computationally inexpensive GGA-type functionals in reproducing the structures of water-loaded zeolites. Clearly, the mere reproduction of experimental data will rarely be the ultimate goal of a computational study. To this end, the benchmarking presented here will help to judge the predictive power (and possible limitations) of previous and future DFT investigations of water adsorption in zeolites and related systems. Such investigations might address a variety of topics related to the structure, bonding, and dynamics of water molecules confined to the pores of crystalline materials.

Acknowledgments: The author is indebted to Dr. Rolf Arvidson and Prof. Andreas Lüttge (Marum) for generous access to the Asgard cluster and further technical support, and to Dr. Johannes Birkenstock for helpful comments on the manuscript. Funding by the Central Research Development Fund (CRDF) of the University of Bremen (Funding line 04 – Independent Projects for Post-Docs) is gratefully acknowledged.

References

[1] A. Di Lella, N. Desbiens, A. Boutin, I. Demachy, P. Ungerer, J.-P. Bellat, A. H. Fuchs, Molecular simulation studies of water physisorption in zeolites. *Phys. Chem. Chem. Phys.* **2006**, *8*, 5396.

[2] D. Bougeard, K. S. Smirnov, Modelling studies of water in crystalline nanoporous aluminosilicates. *Phys. Chem. Chem. Phys.* **2007**, *9*, 226.

[3] F.-X. Coudert, F. Cailliez, R. Vuilleumier, A. H. Fuchs, A. Boutin, Water nanodroplets confined in zeolite pores. *Faraday Discuss.* **2009**, *141*, 377.

[4] E.-P. Ng, S. Mintova, Nanoporous materials with enhanced hydrophilicity and high water sorption capacity. *Microporous Mesoporous Mater.* **2008**, *114*, 1.

[5] S. K. Henninger, F. P. Schmidt, H.-M. Henning, Water adsorption characteristics of novel materials for heat transformation applications. *Appl. Therm. Eng.* **2010**, *30*, 1692.

[6] A. Ristić, N. Z. Logar, S. K. Henninger, V. Kaučič, The performance of small-pore microporous aluminophosphates in low-temperature solar energy storage: the structure-property relationship. *Adv. Funct. Mater.* **2012**, *22*, 1952.

[7] Y. G. Bushuev, G. Sastre, J. V. de Julián-Ortiz, J. Gálvez, Water–hydrophobic zeolite systems. *J. Phys. Chem. C* **2012**, *116*, 24916.

[8] R. X. Fischer, M. Sehovic, W. H. Baur, C. Paulmann, T. M. Gesing, Crystal structure and morphology of fully hydrated zeolite Na-A. *Z. Kristallogr. – Cryst. Mater.* **2012**, *227*, 438.

[9] W. H. Baur, R. X. Fischer, ZeoBase, A new kind of crystal structure database, in: *Proc. 16th Int. Zeolite Conf.*, A. De Frede (ed.), Sorrento, Italy, **2010**.

[10] T. Demuth, L. Benco, J. Hafner, H. Toulhoat, Adsorption of water in mordenite – An ab initio study. *Int. J. Quantum Chem.* **2001**, *84*, 110.

[11] F. Labat, A. H. Fuchs, C. Adamo, Toward an Accurate Modeling of the Water–Zeolite Interaction: Calibrating the DFT Approach. *J. Phys. Chem. Lett.* **2010**, *1*, 763.

[12] S. Quartieri, A. Sani, G. Vezzalini, E. Galli, E. Fois, A. Gamba, G. Tabacchi, One-dimensional ice in bikitaite: single-crystal X-ray diffraction, infra-red spectroscopy and ab-initio molecular dynamics studies. *Microporous Mesoporous Mater.* **1999**, *30*, 77.

[13] E. Fois, A. Gamba, G. Tabacchi, S. Quartieri, G. Vezzalini, On the collective properties of water molecules in one-dimensional zeolitic channels. *Phys. Chem. Chem. Phys.* **2001**, *3*, 4158.

[14] E. Fois, A. Gamba, G. Tabacchi, S. Quartieri, G. Vezzalini, Water molecules in single file: first-principles studies of one-dimensional water chains in zeolites. *J. Phys. Chem. B* **2001**, *105*, 3012.

[15] L. Grajciar, O. Bludský, P. Nachtigall, Water adsorption on coordinatively unsaturated sites in CuBTC MOF. *J. Phys. Chem. Lett.* **2010**, *1*, 3354.

[16] J. Toda, M. Fischer, M. Jorge, J. R. B. Gomes, Water adsorption on a copper formate paddlewheel model of CuBTC: a comparative MP2 and DFT study. *Chem. Phys. Lett.* **2013**, *587*, 7.

[17] A. V. Larin, D. N. Trubnikov, D. P. Vercauteren, Influence of hydrogen bonding on the properties of water molecules adsorbed in zeolite frameworks. *Int. J. Quantum Chem.* **2003**, *92*, 71.

[18] A. V. Larin, D. N. Trubnikov, D. P. Vercauteren, Improvement of X-ray diffraction geometries of water physisorbed in zeolites on the basis of periodic Hartree-Fock calculations. *Int. J. Quantum Chem.* **2005**, *102*, 971.

[19] K. Ståhl, Å. Kvick, S. Ghose, One-dimensional water chain in the zeolite bikitaite: Neutron diffraction study at 13 and 295 K. *Zeolites* **1989**, *9*, 303.

[20] I. A. Belitsky, S. P. Gabuda, W. Joswig, H. Fuess, Study of the structure and dynamics of the water in the zeolite edingtonite at low temperature by neutron diffraction and NMR-spectroscopy, *N. Jahrb. Mineral. Monatsh.* **1986**, *12*, 541.

[21] G. Artioli, R. Rinaldi, Å. Kvick, J. V. Smith, Neutron diffraction structure refinement of the zeolite gismondine at 15 K. *Zeolites* **1986**, *6*, 361.

[22] Å. Kvick, K. Ståhl, A neutron diffraction study of the bonding of zeolitic water in scolecite at 20 K. *Z. Kristallogr. – Cryst. Mater.* **1985**, *171*, 141.

[23] G. Artioli, J. V. Smith, Å. Kvick, Neutron diffraction study of natrolite, $Na_2Al_2Si_3O_{10}\cdot 2H_2O$, at 20 K. *Acta Crystallogr. Sect. C Cryst. Struct. Commun.* **1984**, *40*, 1658.

[24] Å. Kvick, G. Artioli, J. V. Smith, Neutron diffraction study of the zeolite yugawaralite at 13 K. *Z. Kristallogr. – Cryst. Mater.* **1986**, *174*, 265.

[25] S. J. Clark, M. D. Segall, C. J. Pickard, P. J. Hasnip, M. I. J. Probert, K. Refson, M. C. Payne, First principles methods using CASTEP. *Z. Kristallogr. – Cryst. Mater.* **2005**, *220*, 567.

[26] V. Milman, K. Refson, S. J. Clark, C. J. Pickard, J. R. Yates, S.-P. Gao, P. J. Hasnip, M. I. J. Probert, A. Perlov, M. D. Segall, Electron and vibrational spectroscopies using DFT, plane waves and pseudopotentials: CASTEP implementation. *J. Mol. Struct. THEOCHEM* **2010**, *954*, 22.

[27] P. Haas, F. Tran, P. Blaha, Calculation of the lattice constant of solids with semilocal functionals. *Phys. Rev. B* **2009**, *79*, 085104.

[28] J. P. Perdew, A. Zunger, Self-interaction correction to density-functional approximations for many-electron systems. *Phys. Rev. B* **1981**, *23*, 5048.

[29] J. P. Perdew, K. A. Jackson, M. R. Pederson, D. J. Singh, C. Fiolhais, Atoms, molecules, solids, and surfaces: applications of the generalized gradient approximation for exchange and correlation. *Phys. Rev. B* **1992**, *46*, 6671.

[30] J. P. Perdew, K. Burke, M. Ernzerhof, Generalized gradient approximation made simple. *Phys. Rev. Lett.* **1996**, *77*, 3865.

[31] J. Perdew, A. Ruzsinszky, G. Csonka, O. Vydrov, G. Scuseria, L. Constantin, X. Zhou, K. Burke, restoring the density-gradient expansion for exchange in solids and surfaces. *Phys. Rev. Lett.* **2008**, *100*, 136406.

[32] Z. Wu, R. Cohen, More accurate generalized gradient approximation for solids. *Phys. Rev. B* **2006**, *73*, 235116.

[33] B. Hammer, L. B. Hansen, J. Nørskov, Improved adsorption energetics within density-functional theory using revised Perdew-Burke-Ernzerhof functionals. *Phys. Rev. B* **1999**, *59*, 7413.

[34] F. Ortmann, F. Bechstedt, W. Schmidt, Semiempirical van der Waals correction to the density functional description of solids and molecular structures. *Phys. Rev. B* **2006**, *73*, 205101.

[35] S. Grimme, Semiempirical GGA-type density functional constructed with a long-range dispersion correction. *J. Comput. Chem.* **2006**, *27*, 1787.

[36] A. Tkatchenko, M. Scheffler, Accurate molecular van der Waals interactions from ground-state electron density and free-atom reference data. *Phys. Rev. Lett.* **2009**, *102*, 073005.

[37] C. M. Zicovich-Wilson, M. L. San-Román, M. A. Camblor, F. Pascale, J. S. Durand-Niconoff, Structure, vibrational analysis,

and insights into host-guest interactions in as-synthesized pure silica ITQ-12 zeolite by periodic B3LYP calculations. *J. Am. Chem. Soc.* **2007**, *129*, 11512.

[38] J. Ireta, J. Neugebauer, M. Scheffler, On the accuracy of DFT for describing hydrogen bonds: dependence on the bond directionality. *J. Phys. Chem. A* **2004**, *108*, 5692.

[39] D. Tunega, T. Bučko, A. Zaoui, Assessment of ten DFT methods in predicting structures of sheet silicates: Importance of dispersion corrections. *J. Chem. Phys.* **2012**, *137*, 114105.

[40] W. R. Busing, H. A. Levy, The effect of thermal motion on the estimation of bond lengths from diffraction measurements. *Acta Crystallogr.* **1964**, *17*, 142.

[41] K. Momma, F. Izumi, VESTA 3 for three-dimensional visualization of crystal, volumetric and morphology data. *J. Appl. Crystallogr.* **2011**, *44*, 1272.

[42] R. Dovesi, R. Orlando, A. Erba, C. M. Zicovich-Wilson, B. Civalleri, S. Casassa, L. Maschio, M. Ferrabone, M. De La Pierre, P. D'Arco, Y. Noël, M. Causà, M. Rérat, B. Kirtman, CRYSTAL14: A program for the ab initio investigation of crystalline solids, *Int. J. Quantum Chem.* **2014**, *114*, 1287.

[43] L. Rao, H. Ke, G. Fu, X. Xu, Y. Yan, Performance of several density functional theory methods on describing hydrogen-bond interactions. *J. Chem. Theory Comput.* **2009**, *5*, 86.

[44] K. S. Thanthiriwatte, E. G. Hohenstein, L. A. Burns, C. D. Sherrill, Assessment of the performance of DFT and DFT-D methods for describing distance dependence of hydrogen-bonded interactions. *J. Chem. Theory Comput.* **2011**, *7*, 88.

Supplemental Material: The online version of this article (DOI: 10.1515/zkri-2014-1809) offers supplementary material, available to authorized users.